Mon. Not. R. Astron. Soc. **000**, 1–9 (2015) Printed 6 October 2015 (MN LATEX style file v2.2)

A view of Large Magellanic Cloud HII regions N159, N132, and N166 through the 345 GHz window

S. Paron[1,2⋆], M. E. Ortega[1], C. Fariña[3], M. Cunningham[4], P. A. Jones[4], and M. Rubio[5]
[1] *Instituto de Astronomía y Física del Espacio (IAFE), CC 67, Suc. 28, 1428 Buenos Aires, Argentina*
[2] *FADU and CBC, Universidad de Buenos Aires, Argentina*
[3] *Isaac Newton Group of Telescopes, E38700, La Palma, Spain*
[4] *School of Physics, University of New South Wales, Sydney, NSW 2052, Australia*
[5] *Departamento de Astronomía, Universidad de Chile, Casilla 36-D, Santiago, Chile*

arXiv:1510.01246v1 [astro-ph.GA] 5 Oct 2015

Accepted XXXX. Received XXXX; in original form XXXX

ABSTRACT

We present results obtained towards the HII regions N159, N166, and N132 from the emission of several molecular lines in the 345 GHz window. Using ASTE we mapped a $2\farcm4 \times 2\farcm4$ region towards the molecular cloud N159-W in the ^{13}CO J=3–2 line and observed several molecular lines at an IR peak very close to a massive young stellar object. ^{12}CO and ^{13}CO J=3–2 were observed towards two positions in N166 and one position in N132. The ^{13}CO J=3–2 map of the N159-W cloud shows that the molecular peak is shifted southwest compared to the peak of the IR emission. Towards the IR peak we detected emission from HCN, HNC, HCO^+, C_2H J=4–3, CS J=7–6, and tentatively $C^{18}O$ J=3–2. This is the first reported detection of these molecular lines in N159-W. The analysis of the C_2H line yields more evidence supporting that the chemistry involving this molecular species in compact and/or UCHII regions in the LMC should be similar to that in Galactic ones. A non-LTE study of the CO emission suggests the presence of both cool and warm gas in the analysed region. The same analysis for the CS, HCO^+, HCN, and HNC shows that it is very likely that their emissions arise mainly from warm gas with a density between 5×10^5 to some 10^6 cm^{-3}. The obtained $\frac{\rm HCN}{\rm HNC}$ abundance ratio greater than 1 is compatible with warm gas and with an star-forming scenario. From the analysis of the molecular lines observed towards N132 and N166 we propose that both regions should have similar physical conditions, with densities of about 10^3 cm^{-3}.

Key words: galaxies: ISM – (galaxies:) Magellanic Clouds – (ISM:) HII regions – ISM: molecules

1 INTRODUCTION

The Large Magellanic Cloud (LMC), at only 49.97 kpc (Pietrzyński et al. 2013) is a gas rich environment with reduced metallicity (Z about half of the Galactic value) that allow us to obtain detailed observational data to study the physical processes leading to massive star formation in an interstellar medium (ISM) that may be comparable, to certain degree, to those conditions of some star-forming sites in our Galaxy in the early stages (see for example Yamada et al. 2013). Several global surveys of the molecular component in the LMC have been done so far, mainly in the CO J=1–0 emission, in increasing resolutions, starting with an angular resolution of $\sim10'$ (Cohen et al. 1988; Rubio et al. 1991), to the latest made with NANTEN with $2\farcm6$ of angular resolution (Fukui et al. 2008). These surveys were complemented with observations at better angular resolution of known individual cloud complexes, such as the ESO SEST Key Programme (e.g. Israel et al. 1993; Garay et al. 2002; Israel et al. 2003), the Magellanic Mopra Assessment (e.g. Wong et al. 2011), and the second survey of molecular clouds with NANTEN (Kawamura et al. 2009).

Most of the molecular line surveys and individual observations towards the LMC do not cover the 345 GHz window, which contains several molecular lines that provide substantial information about the physical and chemical conditions. With the idea of carry out a comparative study of the physical conditions of the molecular gas in HII regions in the LMC using molecular lines in the 345 GHz windows, we have made observations with the Atacama Submillimetre

⋆ sparon@iafe.uba.ar

© 2015 RAS

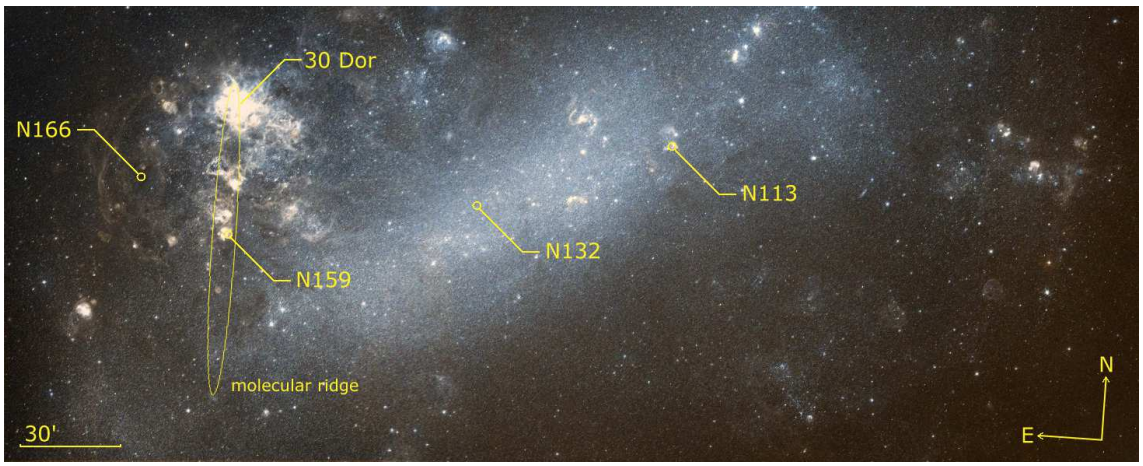

Figure 1. Main area of the LMC in which the location of the HII regions studied in this paper (N159, N132, and N166) and N133 from Paron et al. (2014) are indicated. As reference, 30 Dor and the location of the LMC molecular ridge are also showed. The background is an optical image from DSS Hierarchical Progressive Survey retrieved via Aladin (Bonnarel et al. 2000).

Telescope Experiment (ASTE) towards different regions. In Paron et al. (2014) (hereafter Paper I), we published the results from N113 study. In this paper we add the results from the study of other three HII regions: N159, N132, and N166. Although these regions share the same global characteristics in terms of metallicity, they are located in a completely different environment within the LMC (see Figure 1).

N159 is by far the most studied HII region of the set. Situated approximately 600 pc in projection south of 30 Dor, in the CO molecular ridge, it is a region likely perturbed by the interaction with the Milky Way halo (Ott et al. 2008). The N159 complex was classified, in the NANTEN catalog compiled by Fukui et al. (2008), as a type III giant molecular cloud (GMC), that is a GMC with HII regions and young star clusters. This complex is populated by young massive stars (e.g. Fariña et al. 2009) and presents numerous features characteristic of active star formation regions. Gatley et al. (1981) discovered the first extragalactic protostar here, and Caswell & Haynes (1981) the first Type I extragalactic OH maser. It is known that N159 hosts massive embedded young stellar objects (YSOs), a maser source, and several ultracompact HII regions (Chen et al. 2010). The carbon in the gaseous phase of the whole complex was studied in detail by Bolatto et al. (2008), whereas Mizuno et al. (2010) studied the warm dense molecular gas. Recently Fukui et al. (2015), using ALMA ^{13}CO J=2–1 observations, discovered the first extragalactic protostellar molecular outflows towards this region.

N166 located in projection about 550 pc south-east of 30 Dor, between 30 Dor and N159 to the east of the CO molecular ridge. This region, associated with the molecular cloud DEM 310 (Davies et al. 1976) and the giant molecular Complex-37 (Garay et al. 2002), was cataloged as type II GMC (a GMC with HII regions only) in the NANTEN catalog. Minamidani et al. (2008) studied the ^{12}CO J=1–0 and J=3–2 emission towards five clumps in N166, and suggest that this region is in a younger phase of star formation than N159 as density has not yet reached high enough to start the born of massive stars.

N132 located in projection about 1200 pc south-west of 30 Dor, on the northern edge of LMC bar, is associated with the molecular clouds DEM 172, 173 and 186 (Davies et al. 1976; Kawamura et al. 2009). As in the case of N166 this region is also a GMC Type II. This region has not been particularly studied apart of a global characterization in which the H_2 column density is estimated and the H_2–CO ratio determined (Israel 1997).

In this paper we present the study we have carried out with new observations made towards the LMC HII regions N159, N132, and N166 in a set of molecular lines in the 345 GHz window: ^{12}CO and ^{13}CO J=3–2 and the unexplored lines (in N159) HCN, HNC, HCO^+, and C_2H (in the J=4–3 transition), CS J=7–6, and $C^{18}O$ J=3–2.

2 OBSERVATIONS AND DATA REDUCTION

The molecular observations were performed between July and August 2010 with the 10 m ASTE telescope (Ezawa et al. 2004). The CATS345 GHz band receiver, a two-single band SIS receiver remotely tunable in the LO frequency range of 324-372 GHz, was used. The XF digital spectrometer was set to a bandwidth and spectral resolution of 128 MHz and 125 kHz, respectively. The spectral velocity resolution was 0.11 km s^{-1} and the half-power beamwidth (HPBW) was 22″ at 345 GHz. The system temperature varied from T_{sys} = 150 to 250 K and the main-beam efficiency was $\eta_{mb} \sim 0.65$. The conversion factor to convert from Kelvin to Jansky is 78.3 (from T_A).

The data were reduced with NEWSTAR[1] and the spectra processed using the XSpec software package[2]. The spectra were Hanning smoothed to improve the signal-to-noise ratio, and in some cases, a boxcar smoothing was also applied. Polynomials between first and third order were used for baseline fitting.

Several molecular lines in the 345 GHz window were

[1] Reduction software based on AIPS developed at NRAO, extended to treat single dish data with a graphical user interface (GUI).
[2] XSpec is a spectral line reduction package for astronomy which has been developed by Per Bergman at Onsala Space Observatory.

Table 1. Observed positions.

Region	R.A. (J2000)	Dec. (J2000)
N159	5:39:37.1	−69:45:24.9
N132	5:25:04.1	−69:40:43.6
N166-A	5:44:23.9	−69:26:22.6
N166-B	5:44:36.0	−69:25:28.5

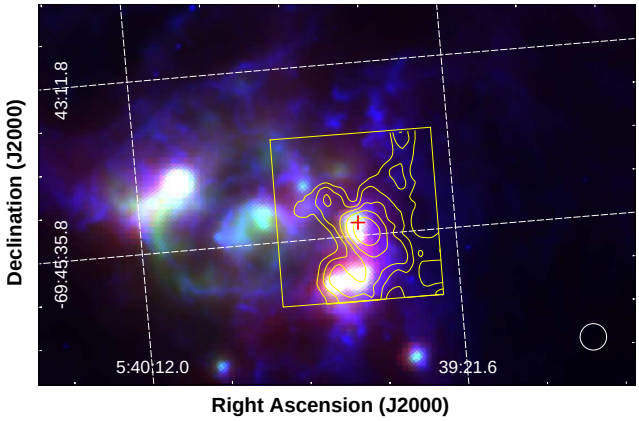

Figure 2. Three-colour image of N159 where the 8, 24, and 70 μm emission toward N159 obtained from the IRAC and MIPS cameras of the Spitzer Space Telescope (from SAGE Spitzer; Meixner et al. 2006) are presented in blue, green, and red, respectively. The yellow box shows the region mapped in the ^{13}CO J=3–2 line with an angular resolution of 22″. The contours correspond to the ^{13}CO J=3–2 emission integrated between 225 and 250 km s^{-1} with levels of 3, 5, 7, 10, and 15 K km s^{-1}. The rms noise is 0.4 K km s^{-1}. The red cross indicates the position where single spectra of several molecular lines were observed. The beam size of the observations is included at the bottom right corner.

observed towards the regions N159, N132, and N166. The observed positions are indicated in Table 1. In the case of N166 two different positions were observed, which are indicated as A and B in the Table. These observations were performed in position switching mode. Additionally, we mapped a 2′.4 × 2′.4 region towards N159 centred at R.A.=5:39:38.3, dec.= −69:45:19.6 (J2000) in the ^{13}CO J=3–2 line. This observation was performed in on-the-fly mapping mode achieving an angular sampling of 6″.

3 RESULTS

Figure 2 is a three-colour image displaying the mid/far-IR emission in the N159 area where the mapped region in the ^{13}CO J=3–2 line is indicated with a yellow square. The ^{13}CO J=3–2 emission integrated between 225 and 250 km s^{-1} is presented in contours. The surveyed region corresponds to the molecular cloud N159-W (Johansson et al. 1998; Bolatto et al. 2000) which hosts several massive young stellar objects (MYSOs) (Chen et al. 2010). Moreover, recently Fukui et al. (2015), using ALMA ^{13}CO J=2–1 observations, discovered the first extragalactic protostellar molecular outflows towards this region.

From the ^{13}CO J=3–2 map of N59-W and by assuming local thermodynamic equilibrium (LTE) we roughly estimate the molecular mass following the same procedure as done in Paper I. From the ^{12}CO J=3–2 peak temperature (see Table 2) we derive an excitation temperature of $T_{ex} \sim 17$ K. Using the peak ^{12}CO and ^{13}CO temperatures ratio, we obtain the optical depths $\tau_{12} \sim 10.5$ and $\tau_{12} \sim 0.2$, which shows that the ^{13}CO J=3–2 line is optically thin. Once obtained the ^{13}CO column density (see Equation 3 in Paper I), we assumed an abundance ratio of $[^{13}CO/H_2] = 5.8 \times 10^{-7}$ (Heikkilä et al. 1999) to derive the H_2 column density. Finally, the molecular mass was estimated from:

$$M = \mu\ m_H \sum_i \left[D^2\ \Omega_i\ N_i(H_2)\right],$$

where Ω is the solid angle subtended by the beam size, D is the distance (50 kpc), m_H is the hydrogen mass, and μ is the mean molecular weight, assumed to be 2.8 by taking into account a relative helium abundance of 25 %. The summation was performed over all the beam positions belonging to the molecular structure delimited by the 7 K km s^{-1} contour displayed in Fig. 2. The obtained mass is $M_{LTE} \sim 3.5 \times 10^4$ $M_\odot$.

Figure 3 shows the spectra of the molecular lines observed towards N159-W (red cross in Fig. 2). This position is about 4″ close to the location of the MYSO 053937.56-694525.4 catalogued in Chen et al. (2010) which is very likely the responsible of the molecular outflows detected by Fukui et al. (2015). Despite the high noise in the C^{18}O J=3–2 line (about 25 mK), we included the spectrum as the signal is still quite evident. Figures 4 and 5 show the CO isotopes spectra observed towards N132 and N166. The line parameters from these spectra are presented in Table 2. The peak main-beam temperature, the central velocity, and the FWHM line width (Cols. 3–5) were obtained from Gaussians fits (red curves in the spectra figures). Col. 6 lists the integrated line intensity. The C_2H J=4–3 line presents two peaks due to its fine structure components. One peak should correspond to the blended C_2H (4–3) J=9/2–7/2 F=5–4 and 4–3 lines, and the other to the blended (4–3) J=7/2–5/2 F=4–3 and 3–2 lines (see Paper I where it is presented the same detection towards N133, and the NIST data base[3]). The HCN J=4–3 emission was fitted with two Gaussians, probably due to a fine structure component, however, in Table 2 the integrated line intensity refers to the entire line.

Table 3 presents the integrated intensity ratios for some of the lines presented in Table 2. For comparison, the ratios obtained towards N159-W from the J=1–0 line by Chin et al. (1997) are also included. Table 3 lists as well the ratios obtained towards N113 from Paper I.

3.1 Non-LTE analysis of N159

Using the ^{12}CO and ^{13}CO J=1–0 line parameters from Chin et al. (1997), the convolved ^{12}CO and ^{13}CO J=2–1 from Johansson et al. (1994), our results of the ^{12}CO and ^{13}CO J=3–2 lines, and the line parameters of ^{12}CO J=4–3 and J=6–5 towards the same position of our observation point at N159-W (T_{mb}^{4-3} = 8 K, Δv^{4-3} = 8.9 km s^{-1} and T_{mb}^{6-5} = 6.6 K, Δv^{6-5} = 7.6 km s^{-1}; data

[3] http://www.nist.gov/pml/data/micro/index.cfm

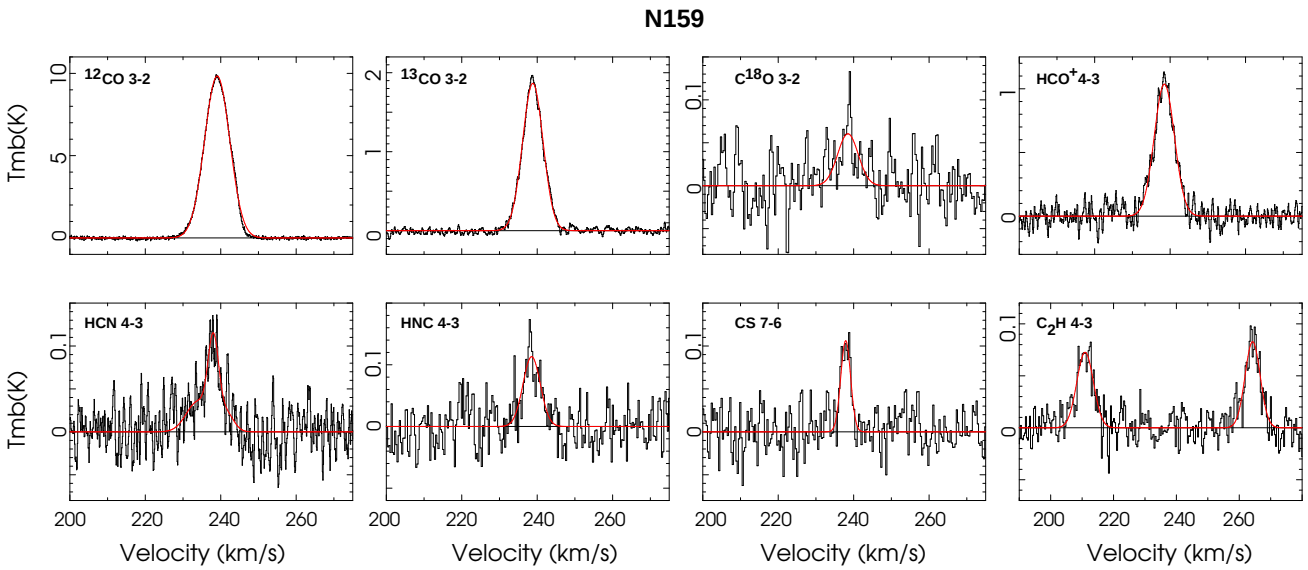

Figure 3. Spectra of the detected molecular lines towards N159-W. The Gaussian fitting to each spectrum is shown in red.

Table 2. Line parameters for the observed molecular lines.

Molecular line	Frequency (GHz)	T_{mb} peak (K)	v_{LSR} (km s^{-1})	Δv (FWHM) (km s^{-1})	$\int T_{mb}dv$ (K km s^{-1})
N159					
^{12}CO (3–2)	345.795	9.83	239.05	7.85	81.7±1.6
^{13}CO (3–2)	330.587	1.86	238.85	6.40	12.7±1.5
C^{18}O (3–2)	329.330	0.05*	235.68	4.73	0.47±0.25
CS (7–6)	342.882	0.11	237.89	3.06	0.37±0.05
C_2H (4–3)	349.399	0.082	237.59	5.66	0.51±0.08
		0.072		6.23	0.49±0.07
HCO$^+$ (4–3)	356.734	1.03	238.47	6.30	7.0±1.2
HCN (4–3)	354.505	0.095	238.10	5.24	0.80±0.10
		0.035	232.70	7.00	
HNC (4–3)	362.630	0.11	238.53	5.42	0.64±0.07
N132					
^{12}CO (3–2)	345.795	4.85	264.55	4.35	22.7±1.2
^{13}CO (3–2)	330.587	0.66	265.00	3.10	2.2±0.5
N166-A					
^{12}CO (3–2)	345.795	3.36	229.47	6.23	22.2±1.4
^{13}CO (3–2)	330.587	0.45	230.22	4.68	2.3±0.4
N166-B					
^{12}CO (3–2)	345.795	5.00	228.05	4.26	23.4±1.3
^{13}CO (3–2)	330.587	0.67	227.93	2.89	2.1±0.4

* The rms noise is 0.025 K.

Table 3. Integrated intensity ratios.

Ratio	N159[a]	N159$^{b}_{(1-0)}$	N113[c]	N113$^{b}_{(1-0)}$	N132[a]	N166-A[a]	N166-B[a]
$\frac{^{12}CO}{^{13}CO}$	6.4 ± 0.7	9.12	6.9 ± 1.1	7.28	10.31 ± 2.40	9.65 ± 1.02	11.14 ± 1.11
$\frac{HCO^+}{HCN}$	8.7 ± 1.8	1.36	4.8 ± 1.1	1.35	–	–	–
$\frac{HCN}{HNC}$	1.25 ± 0.18	3.90	2.0 ± 0.7	2.82	–	–	–
$\frac{HNC}{HCO^+}$	0.09 ± 0.01	0.18	0.10 ± 0.03	0.26	–	–	–

[a] This work.
[b] Ratios from the J=1–0 lines (Chin et al. 1997)
[c] Ratios from the same lines used in this work (Paper I)

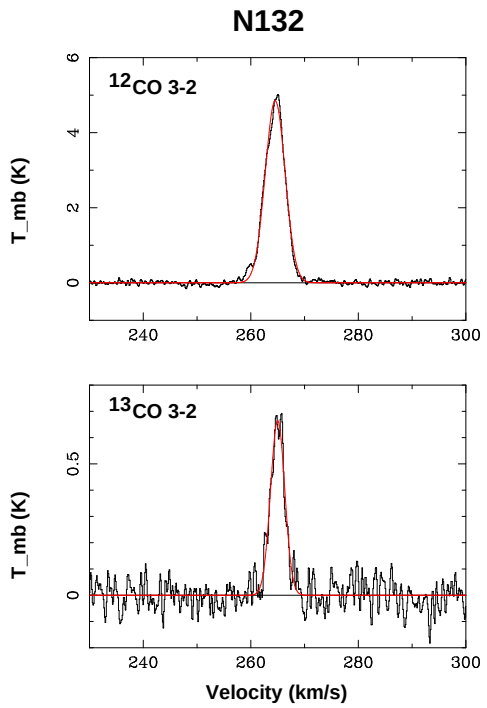

Figure 4. Spectra of the CO isotopes detected towards N132. The Gaussian fitting to each spectrum is shown in red.

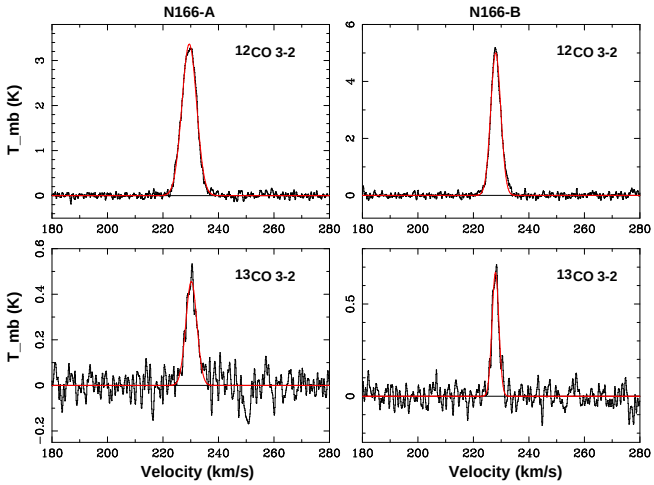

Figure 5. Spectra of the CO isotopes detected towards both positions in N166. The Gaussian fitting to each spectrum is shown in red.

kindly provided by Okada Y., see Okada et al. 2015) we performed a non-LTE study of the CO using the RADEX code (van der Tak et al. 2007). The main-beam temperatures were corrected for beam dilution by calculating $T'_{mb} = T_{mb}/\eta_{bf}$. Following Okada et al. (2015), we used a beam filling factor of $\eta_{bf} = 0.5$. Figure 6 presents the results obtained for kinetic temperatures of 20 and 80 K, displaying the expected H_2 density and the column density pairs corresponding to a given T'_{mb}. The kinetic temperature values are due to consider both the presence of a cold gas component (Ott et al. (2010) obtained a $T_k \sim 16$ K from ammonia lines), and a warmer one (likely due to the star forming processes and the radiation from massive stars). In the warmer case the code was run for a grid of kinetic temperatures between 20 and 100 K. The selected model was that in which the intersection of the curves is more tight (this was the model with $T_k = 80$ K). To perform this analysis, we assumed that the lower CO transitions arise mainly from the cold gas component, while the higher ones from the warmer one. Given that it is likely that the J=3–2 transition arises from both components, a fifty percent of its emission was roughly assigned to each component.

The same non-LTE analysis was done for the CS, HCO^+, HCN, and HNC. The parameters for the lowest transition of these molecular species were obtained from Chin et al. (1997) who observed a point located at $\sim 6''$ from our observation. The results are presented in Figure 7. In the cold gas possibility the results for the HCO^+ do not converge, and in addition, the intersections of all curves are not so tight as in the 80 K case. Table 4 presents the results for all analysed molecules.

4 DISCUSSION

4.1 N159

Our ^{13}CO J=3–2 map of N159-W is very similar to the map recently presented by Okada et al. (2015), which shows that the molecular peak is shifted southwest compared to the peak of the IR emission. It is important to note that we are presenting the first detections of HCO^+, HCN, HNC, and

Table 4. Radex results.

T_k (K)	n_{H_2} (cm^{-3})	N(molec.) (cm^{-2})
	^{12}CO	
20	$(1.1-1.8)\times10^4$	$\sim 2.35\times10^{17}$
80	$(0.1-1.1)\times10^6$	$(4.70-6.23)\times10^{16}$
	^{13}CO	
20	1.32×10^4	$\sim 1.00\times10^{16}$
80	–	–
	CS	
20	4.68×10^6	1.44×10^{13}
80	4.86×10^5	1.28×10^{13}
	HCO$^+$	
20	$>6.3\times10^6$	$(8-9)\times10^{12}$
80	6.76×10^5	8.32×10^{12}
	HCN	
20	5.20×10^6	1.02×10^{13}
80	4.65×10^5	7.74×10^{12}
	HNC	
20	1.25×10^7	2.23×10^{12}
80	3.02×10^6	2.79×10^{12}

Note: $\tau << 1$ in all cases for CS, HCO$^+$, HCN, and HNC. $\tau \sim 1$ and < 1 for most of the cases in ^{12}CO and ^{13}CO. These results are obtained by assuming a beam filling factor of 0.5.

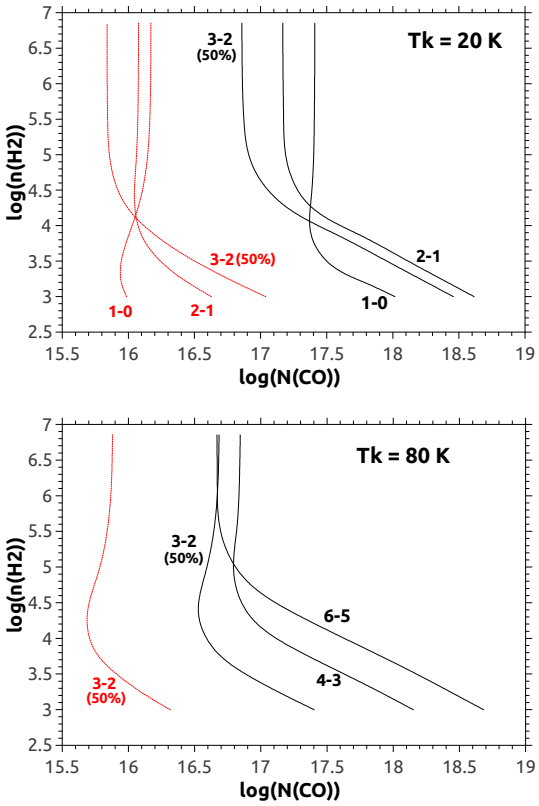

Figure 6. Radex results for ^{12}CO (black lines) and ^{13}CO (red dashed lines). Data of ^{12}CO J=4–3 and 6–5 lines towards the same point of our observations were kindly provided by Okada Y. (Okada et al. 2015). The J=1–0 and 2–1 lines are from Chin et al. (1997) and Johansson et al. (1994), respectively.

C_2H in the J=4–3 transition, CS in the J=7–6, and tentatively the $C^{18}O$ J=3–2 line towards N159-W, precisely towards an IR peak, revealing that this region has the physical conditions needed to excite these lines (for instance the critical densities of HCO$^+$, HCN J=4–3, and CS J=7–6 are 1.8, 8.5, and 2.9 $\times10^6$ cm^{-3}, respectively (Greve et al. 2009)). Concerning to the C_2H J=4–3 line, as done in N113 (Paper I), we analyse the measured FWHM Δv of the peaks and compare with the analysis presented in Beuther et al. (2008) towards a Galactic sample of star-forming regions in different evolutionary stages. The authors showed that the C_2H J=4–3 lines towards ultracompact HII regions are significantly broader (Δv = 5.5 km s^{-1} in average) than those obtained towards infrared dark clouds and high-mass protostellar objects, i.e. sources representing earlier stages in star formation. Our C_2H Δv values are indeed broad, which is consistent with the position of the molecular observation, almost in coincidence with a bright compact radio continuum source at R.A.=5:39:37.48, dec.= −69:45:26.10 (J2000) (Hunt & Whiteoak 1994; Indebetouw et al. 2004), catalogued as a compact HII region likely generated by two O4V/O5V stars (Martín-Hernández et al. 2005). Thus, we are presenting more evidence supporting that the chemistry involving the C_2H in compact and/or UCHII regions in the LMC should be similar to that in Galactic ones.

The comparison between the ratios from higher transition and those obtained from the lower one presented in Table 3 shows the same trend for both N159 and N113, i.e. ratios from J=4–3 are lower than those from J=1–0 except for $\frac{\rm HCO^+}{\rm HCN}$ in both regions. The discrepancy between both ratios is more pronounced in N159 than in N133. On the other side, the $\frac{\rm HCO^+}{\rm HCN}$ ratio in the J=4–3 line in N159 is almost twice the value derived in N113. This may suggest an overabundance of HCO$^+$ in N159 that is not evidenced in the lower line ratio, probably due to line saturation effect. However, as none excitation effects are taking into account in the line ratios, the overabundance statement is far to be conclusive.

The RADEX results suggest the presence of both cool and warm gas in the analysed region. Indeed, the CO emission at the observed position likely arises from both, gas at 20 K with a density about 1.5×10^4 cm^{-3}, and gas at 80 K with densities between 10^5 and 10^6 cm^{-3}. The CO column density in the warm gas component is ~ 5 times lesser than in the colder one. Our results for the warm gas component are in close agreement with what was obtained by Pineda et al. (2008), who used the ^{12}CO and ^{13}CO J=7–6, 4–3 and 1–0 lines, and some lines of [CI] and [CII]. Additionally, the RADEX results for the CS, HCO$^+$, HCN, and HNC indicate that it is very likely that their emissions arise mainly from warm gas with densities between 5×10^5 to some 10^6 cm^{-3}, which is in agreement with the CO warm results.

It is known that the $\frac{\rm HCN}{\rm HNC}$ abundance ratio depends on kinetic temperature (Schilke et al. 1992). From the obtained column densities we derived $\frac{\rm HCN}{\rm HNC}\sim 2.77$, which is compatible with warm gas (T_k between 50 and 100 K)

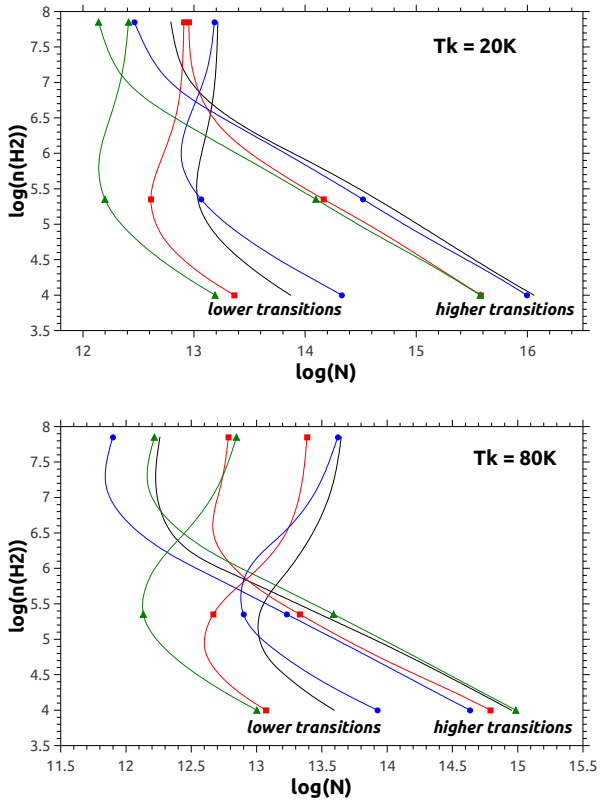

Figure 7. Radex results for CS (black without symbols), HCN (red with squares), HNC (green with triangles), and HCO^+ (blue with circles).

(Helmich & van Dishoeck 1997). In addition, a $\frac{HCN}{HNC}$ ratio greater than 1 agrees with an star-forming scenario (Schöier et al. 2002), and in particular, our value is very similar to the values obtained towards active cores in galactic infrared dark clouds (Jin et al. 2015). The $\frac{HCN}{HNC}$ ratio greater than 1 can be explained by the rapid C + HNC → C + HCN reaction that works as long as the carbon atom abundance is still high (Loison et al. 2014), which seems to be the case, since according to Okada et al. (2015) N159-W has the highest C column density within the N159 complex. This ratio could confirm, in an independent way, the existence of warm gas in the studied region. However, we should be cautious with such ratios because the obtained column densities are dependent on the assumed beam filling factor.

4.2 N132 and N166

In the case of N132 and N166 only ^{12}CO and ^{13}CO were detected. The non-detection of higher density gas tracers such as $C^{18}O$, N_2H^+, and DCO^+ (which were observed in our observation run with integration times of 560 and 1440 sec) may indicate that the density of the molecular gas in these regions is not so high. This is in agreement with what Minamidani et al. (2008) concluded for N166 and is consistent with the higher $^{12}CO/^{13}CO$ integrated intensity ratio compared with the denser regions N159 and N113 (see Table 3). The ratios obtained in N166 are in good agreement with the ratios presented in Garay et al. (2002) using the J=1–0 line for several clouds of the giant molecular Complex-37. N166-A and -B are about 19″ and 27″ close to N166-Clump 2 and N166-Clump 1 belonging to Complex-37 (Minamidani et al. 2008). From an LVG analysis the authors point out that the studied clumps in N166 have a density between some 10^2 to a few 10^3 cm^{-3} with kinetic temperatures between 25 and 150 K. By assuming LTE we obtain similar values of T_{ex} (between 24 and 30 K) and ^{12}CO and ^{13}CO optical depths ($\tau_{12} \sim 7$ and $\tau_{13} \sim 0.14$) for N132 and N166, suggesting that the physical conditions should be similar in both regions.

5 SUMMARY

We have performed a molecular line study towards the LMC HII regions N159, N132, and N166 in the 345 GHz window using ASTE. We mapped a 2′.4 × 2′.4 region towards the molecular cloud N159-W in the ^{13}CO J=3–2 line and several molecular lines as single pointings at an IR peak, about 4″ close to the position of a MYSO. In addition, several molecular lines were also observed towards two positions in N166 and one position in N132, resulting in positive detections only the ^{12}CO and ^{13}CO J=3–2. Our main results can be summarized as follows:

(a) Our ^{13}CO J=3–2 map of N159-W is very similar to the map recently presented by Okada et al. (2015) and shows that the molecular peak is shifted southwest compared to the peak of the IR emission. We estimated the LTE mass of the molecular clump in $\sim 3.5 \times 10^4$ $M_\odot$.

(b) Towards the IR peak position of N159-W we detected emission from HCN, HNC, HCO^+, C_2H J=4–3, CS J=7–6, and tentatively $C^{18}O$ J=3–2, being the first reported detection of these molecular lines in this region. In addition it was obtained an spectrum of ^{12}CO and ^{13}CO J=3–2 towards this position. The detection of the mentioned molecular species in the 345 GHz window proves the presence of high-density gas and shows the usefulness of performing surveys in this wavelength window to increase our knowledge about the physical and chemical conditions of the ISM in the LMC.

(c) The detection and the line width of C_2H J=4–3 towards N159-W is compatible with an environment affected by the action of an HII region. Following our previous study in N113, we conclude that we are presenting more evidence supporting that the chemistry involving this molecular species in compact and/or UCHII regions in the LMC should be similar to that in Galactic ones.

(d) Using our observed CO lines and several lines of this molecule from the literature we performed a non-LTE study which suggests that the CO emission likely arises from both, gas at 20 K with a density about 1.5×10^4 cm^{-3}, and gas at 80 K with densities between 10^5 and 10^6 cm^{-3}. The same non-LTE analysis for the CS, HCO^+, HCN, and HNC shows that we are indeed probing high-density gas (5×10^5 to some 10^6 cm^{-3}) and it is very likely that their emissions arise mainly from warm gas, which is in agreement with the CO warm results.

(e) Using the column densities derived from the non-LTE study we obtained a $\frac{HCN}{HNC}$ abundance ratio greater than 1, which is compatible with warm gas and with an star-forming scenario. This is in agreement with the presence of

MYSOs in the studied region, one of them driving molecular outflows.

(f) Based on the CO line analysis and the non-detection of higher density tracers we suggest that N132 and N166 should have similar physical conditions, with densities between some 10^2 to a few 10^3 cm^{-3} and kinetic temperatures between 25 and 150 K.

ACKNOWLEDGMENTS

We acknowledge the anonymous referee for her/his helpful comments and suggestions. We wish to thank to Y. Okada for kindly provide us with the CO higher transitions data. Thanks to Bastiaan Zinsmeister for his contribution to this paper. The ASTE project is led by Nobeyama Radio Observatory (NRO), a branch of National Astronomical Observatory of Japan (NAOJ), in collaboration with University of Chile, and Japanese institutes including University of Tokyo, Nagoya University, Osaka Prefecture University, Ibaraki University, Hokkaido University, and the Joetsu University of Education. S.P. and M.O. are members of the *Carrera del investigador científico* of CONICET, Argentina. This work was partially supported by grants awarded by CONICET, ANPCYT and UBA (UBACyT) from Argentina. M.R. wishes to acknowledge support from FONDECYT(CHILE) grant N°1140839.

REFERENCES

Beuther, H., Semenov, D., Henning, T., & Linz, H. 2008, ApJL, 675, L33
Bolatto, A. D., Jackson, J. M., Israel, F. P., Zhang, X., & Kim, S. 2000, ApJ, 545, 234
Bolatto, A. D., Leroy, A. K., Rosolowsky, E., Walter, F., & Blitz, L. 2008, ApJ, 686, 948
Bonnarel, F., Fernique, P., Bienaymé, O., et al. 2000, A&AS, 143, 33
Caswell, J. L., & Haynes, R. F. 1981, MNRAS, 194, 33P
Chen, C.-H. R., Indebetouw, R., Chu, Y.-H., et al. 2010, ApJ, 721, 1206
Chin, Y.-N., Henkel, C., Whiteoak, J. B., et al. 1997, A&A, 317, 548
Cohen, R. S., Dame, T. M., Garay, G., et al. 1988, ApJL, 331, L95
Davies, R. D., Elliott, K. H., & Meaburn, J. 1976, MemRAS, 81, 89
Ezawa H., Kawabe R., Kohno K., Yamamoto S., 2004, in Society of Photo-Optical Instrumentation Engineers (SPIE) Conference, Vol. 5489, Society of Photo-Optical Instrumentation Engineers (SPIE) Conference Series, Oschmann Jr. J. M., ed., pp. 763–772
Fariña, C., Bosch, G. L., Morrell, N. I., Barbá, R. H., & Walborn, N. R. 2009, AJ, 138, 510
Fukui, Y., Kawamura, A., Minamidani, T., et al. 2008, ApJS, 178, 56
Fukui, Y., Harada, R., Tokuda, K., et al. 2015, ApJL, 807, L4
Garay, G., Johansson, L. E. B., Nyman, L.-Å., et al. 2002, A&A, 389, 977
Gatley, I., Becklin, E. E., Hyland, A. R., & Jones, T. J. 1981, MNRAS, 197, 17P
Greve, T. R., Papadopoulos, P. P., Gao, Y., & Radford, S. J. E. 2009, ApJ, 692, 1432
Heikkilä, A., Johansson, L. E. B., & Olofsson, H. 1999, A&A, 344, 817
Helmich, F. P., & van Dishoeck, E. F. 1997, A&AS, 124, 205
Hughes, A., Wong, T., Ott, J., et al. 2010, MNRAS, 406, 2065
Hunt, M. R., & Whiteoak, J. B. 1994, Proceedings of the Astronomical Society of Australia, 11, 68
Indebetouw, R., Johnson, K. E., & Conti, P. 2004, AJ, 128, 2206
Israel, F. P., Johansson, L. E. B., Lequeux, J., et al. 1993, A&A, 276, 25
Israel, F. P. 1997, A&A, 328, 471
Israel, F. P., Johansson, L. E. B., Rubio, M., et al. 2003, A&A, 406, 817
Jin, M., Lee, J.-E., & Kim, K.-T. 2015, ApJS, 219, 2
Johansson, L. E. B., Olofsson, H., Hjalmarson, A., Gredel, R., & Black, J. H. 1994, A&A, 291, 89
Johansson, L. E. B., Greve, A., Booth, R. S., et al. 1998, A&A, 331, 857
Kawamura, A., Mizuno, Y., Minamidani, T., et al. 2009, ApJS, 184, 1
Loison, J.-C., Wakelam, V., & Hickson, K. M. 2014, MNRAS, 443, 398
MacLaren, I., Richardson, K. M., & Wolfendale, A. W. 1988, ApJ, 333, 821
Martín-Hernández, N. L., Vermeij, R., & van der Hulst, J. M. 2005, A&A, 433, 205
Meixner, M., Gordon, K. D., Indebetouw, R., et al. 2006, AJ, 132, 2268
Minamidani, T., Mizuno, N., Mizuno, Y., et al. 2008, ApJS, 175, 485
Minamidani, T., Tanaka, T., Mizuno, Y., et al. 2011, AJ, 141, 73
Mizuno, Y., Kawamura, A., Onishi, T., et al. 2010, PASJ, 62, 51
Okada, Y., Requena-Torres, M. A., Güsten, R., et al. 2015, A&A, 580, A54
Ott, J., Wong, T., Pineda, J. L., et al. 2008, PASA, 25, 129
Ott, J., Henkel, C., Staveley-Smith, L., & Weiß, A. 2010, ApJ, 710, 105
Paron, S., Ortega, M. E., Cunningham, M., et al. 2014, A&A, 572, A56
Pietrzyński, G., Graczyk, D., Gieren, W., et al. 2013, Nature, 495, 76
Pineda, J. L., Mizuno, N., Stutzki, J., et al. 2008, A&A, 482, 197
Roberts, H., van der Tak, F. F. S., Fuller, G. A., Plume, R., & Bayet, E. 2011, A&A, 525, A107
Rubio, M., Garay, G., Montani, J., & Thaddeus, P. 1991, ApJ, 368, 173
Schilke, P., Walmsley, C. M., Pineau Des Forets, G., et al. 1992, A&A, 256, 595
Schöier, F. L., Jørgensen, J. K., van Dishoeck, E. F., & Blake, G. A. 2002, A&A, 390, 1001
van der Tak, F. F. S., Black, J. H., Schöier, F. L., Jansen, D. J., & van Dishoeck, E. F. 2007, A&A, 468, 627
Wong, T., Hughes, A., Ott, J., et al. 2011, ApJS, 197, 16

Yamada, S., Suda, T., Komiya, Y., Aoki, W., & Fujimoto, M. Y. 2013, MNRAS, 436, 1362